A Positron-Emission Transaxial Tomograph for Nuclear Imaging (PETT)[1]

Michel M. Ter-Pogossian, Ph.D., Michael E. Phelps, Ph.D., Edward J. Hoffman, Ph.D., and Nizar A. Mullani

An apparatus was developed for obtaining emission transaxial images of sections of organs containing positron-emitting radiopharmaceuticals. The detection system is a hexagonal array of 24 NaI(Tl) detectors connected to coincidence circuits to achieve the "electronic" collimation of annihilation photons. The image is formed by a computer-applied algorithm which provides quantitative reconstruction of the distribution of activity. Computer simulations, phantom and animal studies show that this approach is capable of providing images of better contrast and resolution than are obtained with scintillation cameras. Advantages of positron *vs.* single photon reconstruction tomography are discussed.

INDEX TERMS: Computers • Positron Imaging • Radionuclide Imaging, apparatus and equipment • Radionuclide Imaging, technique • Tomography, radionuclide

Radiology 114:89–98, January 1975

Current methods of nuclear medicine imaging of organs containing gamma-emitting radionuclides impose three major limitations on the usefulness of these techniques. (*a*) Image contrast is severely reduced by activity contained in tissues surrounding the region of interest. This activity, which contributes noise to the image, may vary spatially and temporally, and is often so pronounced that only structures with a high radionuclide concentration can be differentiated from their surroundings. (*b*) In spite of the relatively high inherent resolution capabilities of certain nuclear medicine imaging devices, their effective resolution is limited by that of the collimator whose improvement must be weighed against the concomitant severe loss in detection efficiency. Since the resolution and sensitivity for the imaging of sources in tissues of collimators varies with distance, the perceptibility of small or low contrast structures is usually reduced with depth. (*c*) The widespread use of ^{99m}Tc in nuclear medicine limits the scope of this discipline. Although ^{99m}Tc is readily available, inexpensive, has a low energy-high photon yield, and possesses some desirable chemical properties, there are two drawbacks to its use: (*i*) Because of the low energy of the gamma radiation of ^{99m}Tc, detection efficiency varies significantly with depth and may be affected by the presence of bone overlying the organ of interest, and (*ii*) the chemical properties of ^{99m}Tc are less akin to physiological processes than those of many other radionuclides.

As a consequence of the above limitations, imaging in nuclear medicine has been primarily limited to morphological examinations. While these are undeniably important, potentially rewarding physiological studies which should be possible in this field have been greatly restricted.

We have developed an apparatus which provides high contrast transaxial tomographic images of organs and structures containing positron-emitting radionuclides. This device improves contrast by minimizing the interference from surrounding tissue through the use of annihilation coincidence detection[2] and mathematical reconstruction of cross-section images from a series of views obtained at a number of discrete angles. The resolution achieved is uniform and independent of the depth of the region examined. In addition, since many positron-emitting radionuclides can be used to label not only agents for morphological studies but also biologically active compounds, there are numerous potential applications for this device in nuclear medicine.

METHODS

The concept of reconstructing a tomographic section from the external detection of gamma-ray-emitting radionuclides at multiple angles around a subject has been previously described. Kuhl and

[1] From the Division of Radiation Sciences, Washington University School of Medicine, St. Louis, Mo. Presented at the Sixtieth Scientific Assembly and Annual Meeting of the Radiological Society of North America, Chicago, Ill., Dec. 1–6, 1974.

This work was supported by NIH Grant No. 5 P01 HL13851, by NIH Grant 1 R01 HL15432, and by NIH Fellowship No. 1-F03-GM55196.

[2] The term annihilation coincidence detection in this text denotes the simultaneous detection of the two 511 keV photons which are created by the annihilation of a positron.

ah

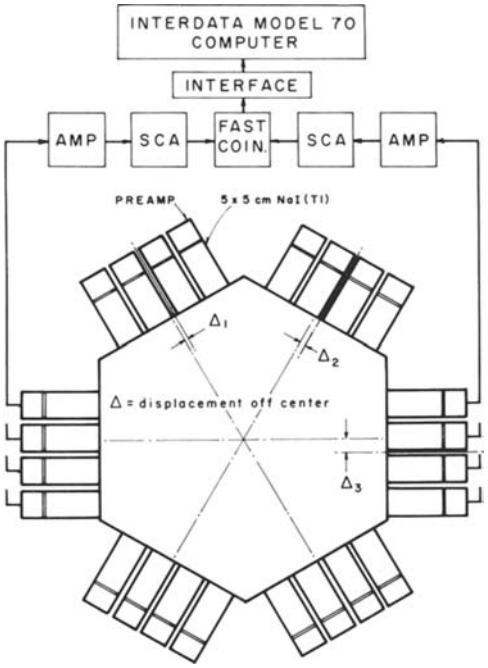

Fig. 1. Schematic diagram of prototype PETT.

his coworkers (21–24) have developed a method of reconstructing a transaxial tomographic section of the head from a series of rectilinear scans performed with scintillation detectors of conventional design. This approach has been applied with modifications by others (3, 27, 31–34). Recently, Budinger (8) described transaxial reconstructions from measurements taken as a subject is rotated within the field of view of a scintillation camera.

The advantages of annihilation coincidence detection in nuclear medicine imaging have also been investigated (6, 7, 9, 14, 25, 35). Brownell and his coworkers (6, 9) successfully developed a camera for the imaging of structures containing positron-emitting radionuclides. The device has also been utilized for tomographic reconstruction with rotation of the object under study (11). Chesler (10, 11) and Cormack (13) pointed out the advantages of annihilation coincidence detection in transaxial tomographic reconstruction. Robertson *et al.* (29) described a tomographic system for positron-emitting nuclides, based on the use of a ring of scintillation detectors operated in the coincidence mode.

We have designed, built, and tested an experimental version of an apparatus which incorporates some of the features of Kuhl's device and a positron detection system similar to that developed by Brownell. However, our system embodies some important characteristics not found in the devices developed by the above investigators. We call this apparatus a *p*ositron *e*mission *t*ransaxial *t*omograph (PETT).

The prototype PETT basically consists of 24 NaI(Tl) scintillation detectors placed in a hexagonal array (Figs. 1 and 2). Each opposing pair of detectors is connected in coincidence such that events are accepted only when two photons are recorded by the two detectors simultaneously. The subject under study is placed on a computer-controlled rotating platform in the center of the hexagon. The data collected from the 12 pairs of detectors are used to reconstruct an image of the cross-section distribution of activity by a computer-applied algorithm.

Coincidence Detection of Annihilation Radiation: The PETT scanner is designed exclusively for use with positron-emitting radionuclides. There are five reasons for this choice. (*a*) Because the annihilation photons are simultaneously emitted at 180°, annihilation coincidence can be used as an "electronic" collimator to limit the field of view to activity lying in a well defined cylinder between the two detectors. This eliminates the need for

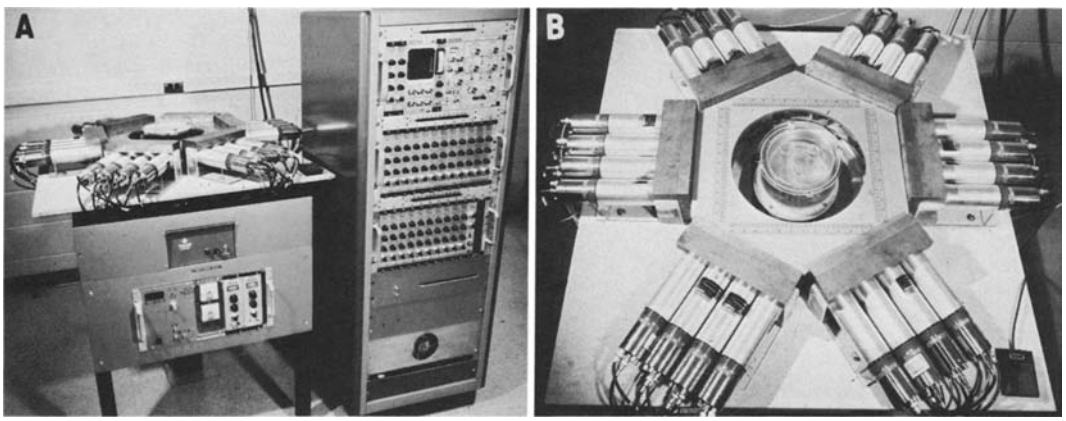

Fig. 2. A. Photograph of prototype PETT. The object examined (phantom or animal) is placed on a turntable at the center of the hexagon. The turntable rotates under computer control, with its axis of rotation perpendicular to the plane of the hexagon.
B. Phantom is shown on the turntable.

absorbing-type collimators. (*b*) The use of annihilation coincidence detection results in higher overall resolution and contrast than are presently available in single photon imaging devices. (*c*) In contrast to the isosensitivity response of single photon detection, the response of annihilation coincidence detection is more uniform and therefore more suited to the interactive relationships of the mathematical reconstruction necessary for tomographic imaging. (*d*) The sensitivity of detection with annihilation coincidence counting is independent of the depth of the activity in tissue. (*e*) "Electronic" collimation allows a much higher radiation detection efficiency without loss in resolution than is possible with conventional collimators. These characteristics of annihilation coincidence detection are discussed in greater detail below in the light of their impact on tomographic reconstruction.

Figure 3 shows the line-spread function (LSF) and the isoresponse curves for a positron-emitting line source in water between two scintillation detectors operated in coincidence. The full width at half maximum (FWHM) of the LSF is about 40% of the exposed diameter of the detector crystals, and it does not vary significantly as a function of the position of the source of radiation between the detectors. In contrast, the resolution of detectors with the typical absorbing collimators used for single photon detection varies

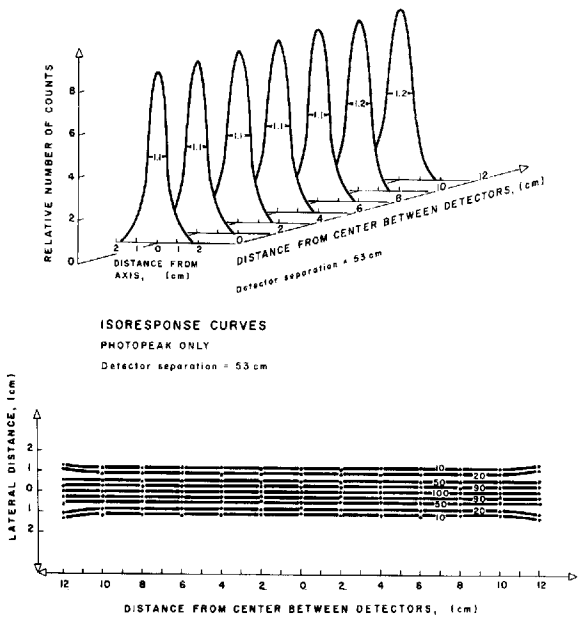

Fig. 3. Line-spread functions (LSF) and isoresponse curves for a positron-emitting line source (^{64}Cu) in water for two opposing scintillation detectors operated in coincidence. The detector crystals are NaI(Tl) cylinders 5.1 cm in diameter and 5.1 cm thick, collimated each with a 2.5-cm straight-bore hole provided in a 2.5-cm-thick lead plate.

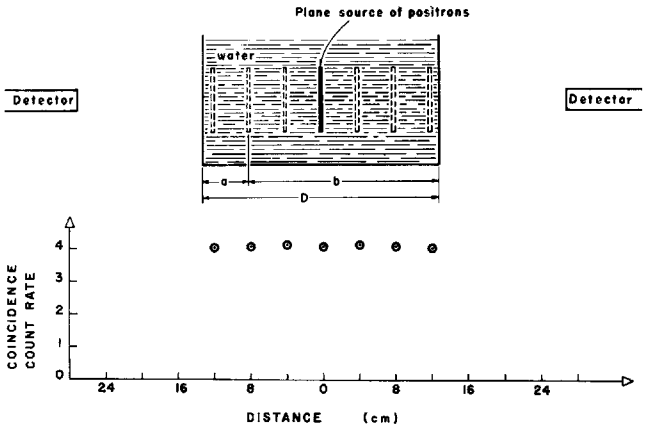

Fig. 4. Depth independence of annihilation coincidence detection. The lower portion of the figure shows coincidence counting rate as a plane radioactive source containing a positron emitter is moved between two detectors. If one annihilation photon traverses the thickness a to reach the detector, the other photon must traverse the thickness b and the attenuation for a coincidence event is contributed by $a + b = D$.

substantially with the distance between the detector and the source. Although some degree of uniformity in the isoresponse curves of single photon detection can be obtained at the expense of efficiency by suitably designed collimators (1, 12, 15), this method does not achieve the uniformity of response provided by annihilation coincidence detection (5, 15, 25, 35).

Annihilation coincidence detection permits the detection of radionuclides with sensitivity independent of depth. As shown in Figure 4, the coincidence count rate remains constant as a plane source containing a positron-emitting radionuclide (^{64}Cu) is moved from one side of a water phantom to the other. This is due to the fact that the two 511-keV annihilation photons must always cross a total path length, D, to be detected in coincidence. The absolute sensitivity can be calculated from D and the attenuation coefficient of the material traversed. This is not the case with single photon detection, where sensitivity decreases with depth due to the increasing path length through the object and corresponding increase in attenuation. Furthermore, the variation in geometrical response of conventional absorbing collimators compounds the difficulty in defining the spatial sensitivity. The high energy of the annihilation radiation (511 keV) also minimizes variations in the attenuation of this radiation in tissues of different composition and thickness.

A fundamental difference between the "electronic" collimation possible with annihilation radiation and conventional absorbing-type collimation used for single photon detection is that the former permits a higher overall radiation detection efficiency when multiple detector systems are

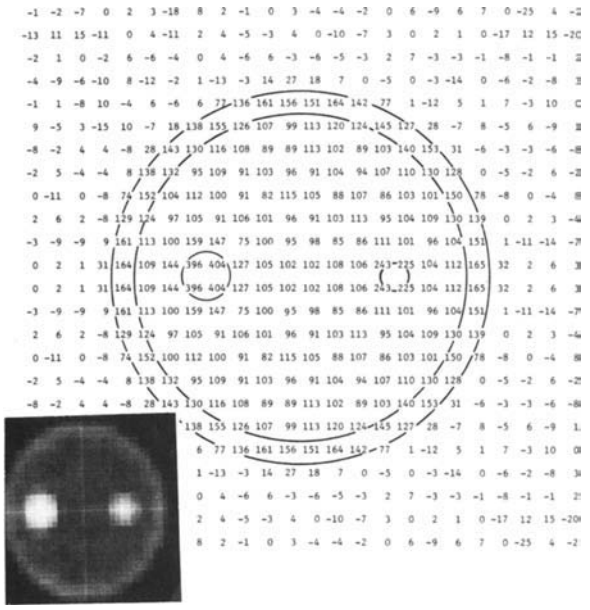

Fig. 5. Numerical printout of PETT reconstructed image from computer-simulated data. Angular and transverse sampling: 7.5° and 1 cm, respectively. The simulated phantom consists of four compartments: a 1-cm-thick outer ring, a 14-cm-diameter inner cylinder, and two cylindrical tubes respectively 2.2 and 1.2 cm in diameter, with simulated activity levels of 2, 1, 4, and 4 in each compartment.
Insert: reconstructed image.

employed.[3] As pointed out by Burnham and Brownell (9), when coincidence collimation is used, all the radiation (neglecting attenuation) can theoretically be detected and its origin established. The lower sensitivity of single-photon detection is inherent to the loss of radiation by absorption in the collimator. The efficiency of single-photon detection systems using multiple detectors increases *directly* with the number of detectors, whereas annihilation coincidence systems composed of multiple detectors can be designed to increase efficiency by the *square* of the number of detectors[3]. Comparisons of sensitivity of single photon and positron detection for dual probe scanners (2, 25) are invalid for larger arrays of detectors which use such a multiple coincidence design unless the above effect is considered.

Reconstruction Algorithm: A number of different reconstruction algorithms have been described for transaxial tomographic section imaging. These algorithms can be broadly classified as Fourier- or non-Fourier-based. The Fourier-based algorithms (4, 10, 28, 30) use Fourier transforms, Fourier series, convolution, or, equivalently, filtering of the collected data to perform the reconstruction. Non-Fourier-based reconstruction algorithms (16–18, 20) in general use algebraic or iterative numerical processing of the data.

We have chosen to use a Fourier-based approach developed by the Biomedical Computer Laboratory, Washington University School of Medicine. The algorithm employed will not be discussed in detail, but some of the general assumptions and criteria of the mathematical reconstruction used in transaxial emission tomography and how they relate to the method of detection will be considered.

The purpose of transaxial reconstruction tomography is to reproduce the distribution of activity in a cross-section slice of the body. The data for reconstruction are a series of activity profiles obtained by performing transverse scanning at various angles about the object in the plane of the cross section of interest. The data collected are used to generate enough independent equations to reconstruct the distribution of activity. One of the primary assumptions in the reconstruction algorithm is that the number of counts recorded at each point represents the sum of the activity along a well defined line (or region) in the plane of interest. This assumption is valid for the well defined and depth-independent response of an annihilation coincidence detection system. However, the varying response with depth of single-photon counting systems violates this assumption, producing a distortion of the image.

Although the attenuation of radiation is constant with respect to depth on a line between two detectors in annihilation coincidence, varying thicknesses of material are interposed between each detector pair as data are collected at different points across the object. Thus an attenuation correction must be made on each data point recorded. One method is to determine the physical dimensions of the object and multiply each data point by $e^{\mu x}$, where x is the thickness of the object between the coincidence detector pairs, and μ is an average linear attenuation coefficient. This approach is subject to error if μ varies significantly across the object, as when the lungs or bone are traversed. Another method consists of measuring the attenuation of 511-keV radiation in the subject and then using this information to correct the emission data before reconstruction. We have used this approach by placing a thin plastic ring containing a solution of ^{64}Cu around the subject and collecting the count rate as a function of transverse and angular position. The same measurement is made without the subject in position, and the ratio of the two measurements gives the

[3] A detailed study of the advantages of positron-emitting radionuclides for tomographic reconstruction is included in "The application of annihilation coincidence detection to transaxial reconstruction tomography" by M. E. Phelps *et al.* (27*a*).

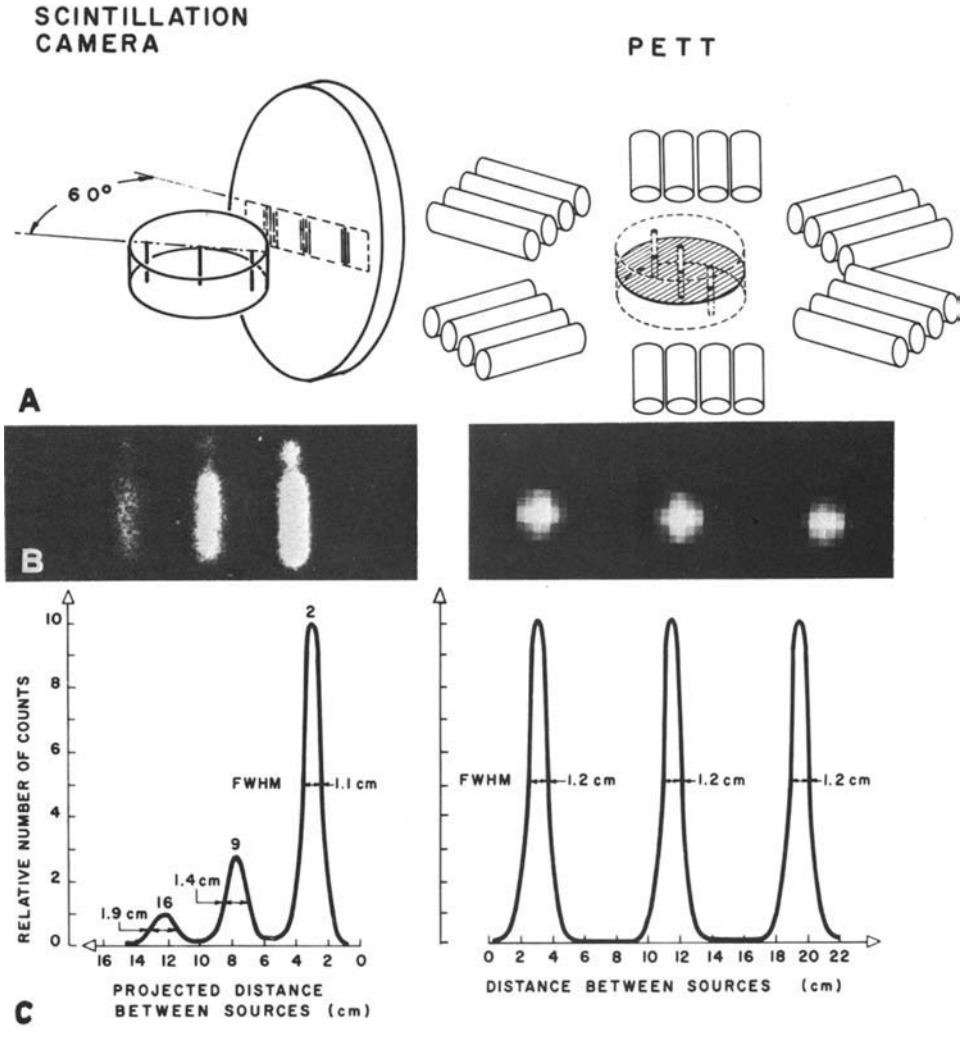

Fig. 6. Comparison of line-spread functions for a scintillation camera (Nuclear Chicago HP with 15,000-hole high-resolution collimator) (left) and for the PETT (right) at various depths in a water phantom. A. Diagram of the placement of the phantom.
B. Recorded images.
C. Line-spread functions *versus* depth. ^{99m}Tc and ^{64}Cu, respectively, were used with the scintillation camera and the PETT.

attenuation factor. Because of the well defined and depth-independent response of annihilation coincidence, this attenuation correction method is accurate and simple to implement.

The reconstruction algorithm used in this study was evaluated by performing reconstructions of computer-simulated phantom data. The results of such a study are shown in Figure 5. The numerical values are in good agreement with the actual values of the activities in the cylinder and the 2.2-cm hot tube. However, the values for the 1-cm thick ring and 1.2-cm hot tube of about 150 and 240 are lower than the correct values of 200 and 400. This is explained by the fact that the sampling resolution, ring, and hot tube dimensions were all about 1 cm, and from the sampling theorem the exact answer can be recovered only if the sampling resolution is $\leq 1/2$ the object size.[4]

The Prototype PETT: A schematic illustration and photographs of the prototype PETT are shown in Figures 1 and 2. The detector consists of twenty-four 5.1 × 5.1-cm NaI(Tl) scintillation detectors placed in a hexagonal array (4 to a side). Lead shields 2.5 cm thick with 2.5-cm diameter straight-bore holes are placed in front of each detector to increase the inherent detector resolution to about 1.1 cm full width at half maximum (FWHM, Fig. 3). Shielding is provided to exclude radiation originating outside the cross section examined. The output of each detector is connected to individual preamplifiers, amplifiers, and single-channel pulse-height analyzers. The output of the single-channel pulse-height analyzers of each directly opposing pair of detectors is connected to a coincidence circuit with a resolving time of 30 nanoseconds (Fig. 1). This establishes the "electronic" collimation of the 12 sets of detectors, since an event is accepted only when two photons are recorded by detectors simultaneously. With the above resolving time and shielding, the random coincidence rate of the data collected in this work for the highest counting rates was less than 5% of the true coincidence rate.

[4] Experimentally, the necessary sampling resolution is usually from 1/2 to 1/4 the object size if quantitative recovery is to be expected.

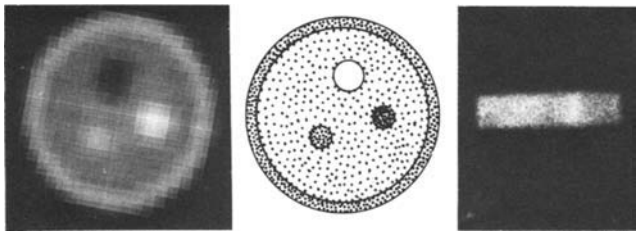

Fig. 7. Comparison of images of a phantom obtained with the PETT (left) and a scintillation camera operated in the conventional mode (same as in Fig. 6) (right). The phantom consists of the following compartments: a 1-cm-thick ring surrounding a 14-cm-diameter cylinder, the latter containing three cylindrical compartments, two of them 2 cm in diameter and the third 3 cm in diameter. The compartments were filled with a radionuclide with relative activities of 3, 1, 5, 3, and 0, respectively. The scintillation camera image was obtained by filling the phantom compartments with a solution of ^{99m}Tc, and the PETT image was obtained with identical activities of ^{64}Cu. Both images were formed by 300,000 counts.

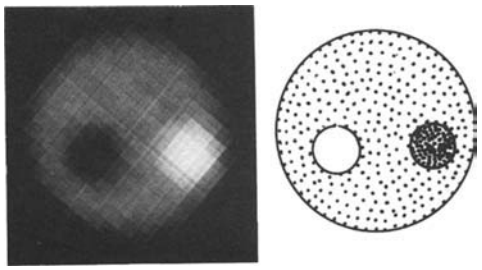

Fig. 8. Test of quantitative reconstruction accuracy of the PETT. Right: Illustration of activity distribution (^{64}Cu) in a 14-cm diameter phantom. Left: Reconstruction image from the PETT. Image formed by 340,000 counts.

The outputs of the 12 coincidence units are routed into a parallel channel interface to an Interdata Model 70 minicomputer.

Each set of four detectors directly faces the four on the opposite side. The detectors are not centered on the side of the hexagon, but are displaced by 0.5Δ, 1.5Δ, and 2.5Δ, where Δ = 1/6 center-to-center distance between neighboring detectors, as shown in Figure 1. After the system rotates 360°, each set of detectors will have recorded data at the same set of angles as all the other sets of detectors. The net result is a set of transverse scans which sample in 24 positions with a sampling resolution of 1 cm. When data are recorded over 360°, it would appear that the second 180° is redundant, since the detectors record activity across the total width of the organ. However, because each set of four coincident pairs of detectors is offset in one direction, there are three displaced sets of data in the rotation from 0° to 180°, and three more complementary displaced sets of data in the 180° to 360° rotation, yielding a total of six independent sets of displaced detector positions.

In the prototype PETT, the object examined is placed on a platform in the center of the 24-detector hexagonal array (Fig. 2). The rotation of the platform is computer-controlled. Coincidence data from the 12 coincident pairs of detectors are recorded every 7.5°, stored, sorted, and then processed by the reconstruction algorithm, using the Interdata Model 70 minicomputer. The data-processing time of the Fourier transform reconstruction algorithm is about 25 seconds. All of the programs are presently written in FORTRAN because of ease of programming. FORTRAN, however, is slower in execution time than the Interdata assembly language. The assembly language version of the algorithm should yield a considerably faster reconstruction calculation.

RESULTS

Phantom Studies: To evaluate the overall resolution of the PETT, three capillary tubes 1.2 mm in diameter, containing a solution of ^{64}Cu, were placed in an 18-cm-diameter cylindrical phantom filled with water (Fig. 6). The data were corrected for attenuation by measuring the thickness of the phantom and applying the attenuation coefficient of water for 511 keV radiation. The reconstructed image containing 200,000 counts and LSFs is shown in Figure 7. For comparison, the same phantom containing ^{99m}Tc was placed against the face of a Nuclear Chicago HP scintillation camera fitted with a high-resolution 15,000-hole collimator. The phantom was oriented such that the line sources formed an angle of 60° with respect to the face of the camera (Fig. 6). The projected distances between the line sources were 4.8 cm. The line sources were 2, 9, and 16 cm from the face of the gamma camera, and 200,000 counts were collected. Numerical data from the scintillation camera were collected in a 32 × 32 array with a PDP-12 computer and used to construct the LSFs for the scintillation camera. This illustrates the decrease in sensitivity and resolution with distance for the scintillation camera and the depth independence of the resolution with the PETT. It can be seen from Figures 3 and 6 that the LSFs for the reconstructed image are in good agreement with the coincident detector response.

In a comparison of the imaging capabilities of the PETT and of a scintillation camera used in the conventional non-tomographic mode (Fig. 7), the PETT image provided better recognition of the phantom structure. Both images contained about 300,000 total counts, collected in 12 minutes by the scintillation camera.

The ability of the PETT to yield a quantitative image was tested (Fig. 8) with a phantom filled with relative activities of 1, 4, and 0 in the cylinder and two 3-cm tubes, respectively. The reconstructed activities were 1 ± 0.1, 4 ± 0.1, and 0 ±

TABLE I: COMPARISON OF DATA COLLECTION TIMES OF A SCINTILLATION CAMERA* AND THE PETT SCANNER FOR A PHANTOM WITH VARIOUS ACTIVITY DISTRIBUTIONS

Phantom†	Total Activity‡ (μCi)	Total No. of Counts in Image	Data Collection Time (min.)	
			Scintillation Camera	PETT
A	370	280,000	15	12
B	600	440,000	16	12
C	480	350,000	14	12

* Nuclear Chicago Model HP fitted with a 15,000-hole high-resolution collimator.

† The phantom consists of a Lucite cylinder approximately 17 cm in external diameter and 10 cm high, filled with a solution of either ^{99m}Tc or ^{64}Cu. Various cylindrical containers with different activities are placed in the phantom.

‡ ^{99m}Tc for the scintillation camera and ^{64}Cu for the PETT.

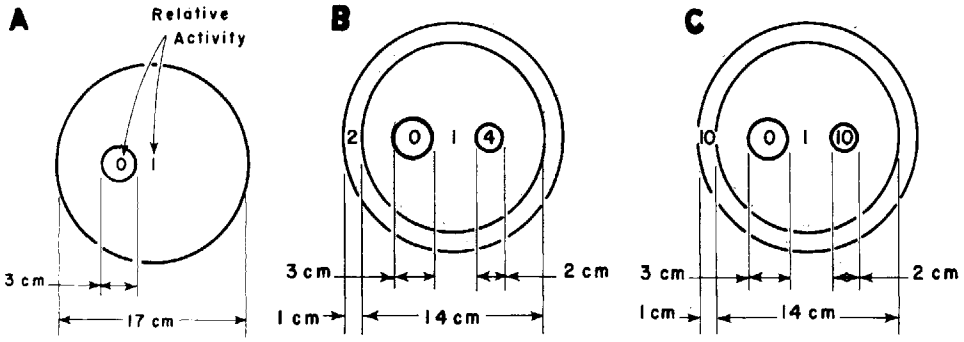

0.1 in the cylinder and the two 3-cm tubes, which is in agreement with the relative activities in the phantom. The 3-cm objects were employed to demonstrate the quantitative aspect of the reconstruction, since the sampling resolution (1.2 cm FWHM) must be 2 to 4 times smaller than the object size (3 cm) for quantitative reconstruction.

The sensitivity of the PETT for imaging purposes was compared to that of the scintillation camera. The data collection times required by the two devices to obtain images of a comparable number of counts are given in TABLE I. Equivalent activities of ^{64}Cu and ^{99m}Tc were employed for the PETT and scintillation camera imaging. It should be noted that while the data were obtained with a phantom filled to the top (7 cm high), the PETT utilized only a cross-section slice slightly thicker than 1 cm for the formation of the image, whereas the scintillation camera collected data from the whole phantom.

Animal Studies: Two sets of experiments were carried out in two dogs (one set per dog) to assess the PETT imaging capabilities for different organs visualized by means of pharmaceuticals labeled with positron-emitting radionuclides. The dogs were 50-lb. mongrels which were anesthetized throughout the duration of the experiment. For each study the dog was placed on the rotating table in the center of the PETT. Data were collected every 7.5° for a 360° rotation. Before each measurement the previously injected activity was allowed to decay to a negligible level for imaging.

In the first set of experiments, positron-emission transverse tomographic sections of the thorax were obtained at the level of the sixth thoracic vertebra (Fig. 9). The experiment was carried out in the following sequence: (*a*) The dog was injected intravenously with 10 mCi of $H_2{}^{15}O$ (^{15}O; $T_{1/2}$ = 2 min.). Three minutes was allowed for equilibration with fast equilibrating water compartments, and an image was obtained in 4.8 minutes. (*b*) Twelve millicuries of $^{13}NH_3$ (^{13}N; $T_{1/2}$ = 10 min.) was injected intravenously and eight minutes was allowed for the clearance of the ammonia from the blood and for equilibration with soft tissues. An image was obtained in 12 minutes. (*c*) The dog was allowed to breathe ^{11}CO (^{11}C; $T_{1/2}$ = 20 min.) for about one minute to label its blood with an estimated 8 mCi of ^{11}CO-hemoglobin. Five minutes was allowed for blood equilibration before a 24-minute data collection period. (*d*) Ten millicuries of ^{18}F ($T_{1/2}$ = 110 min.) in water solution was injected, and a period of one hour was allowed for the fluorine to clear from the blood. The data collection time was 24 minutes.

The images obtained in the above set of experiments were corrected for attenuation by the measured transmission method described above. A transmission image using the data employed for attenuation correction is shown in Figure 9. The image obtained with $H_2{}^{15}O$ shows the distribution of equilibrated water in soft tissues. The equilibration of water in bone is slow, which accounts for a void in the image at the position of the vertebral column. Lungs also show a relatively

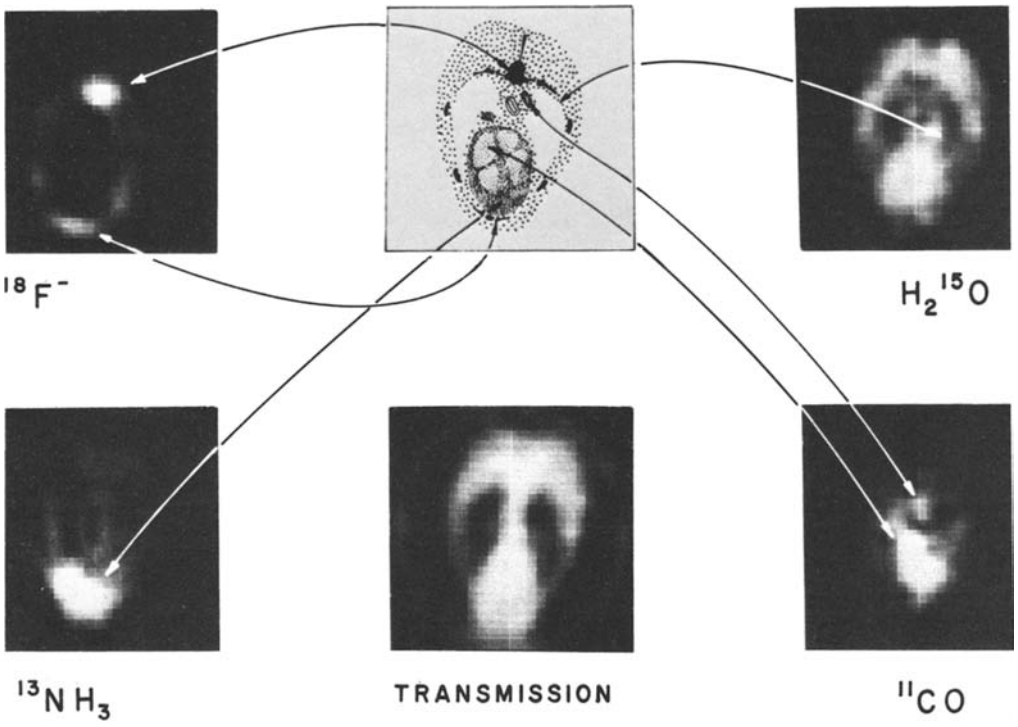

Fig. 9. Cross-section images obtained with the PETT of a dog injected successively with $H_2{}^{15}O$, $^{13}NH_3$, ^{11}CO, and ^{18}F containing 63,000, 230,000, 350,000, and 413,000 counts, respectively. The level of the cross section is at the sixth thoracic vertebra. Anatomical structures at this level are shown at top center. A transmission image reconstructed from the data used for the attenuation correction is shown at the bottom center.

low concentration of $H_2{}^{15}O$. The $^{13}NH_3$ is preferentially taken up in the myocardium, as reported by others (19, 26). The contrast ratio between the myocardium and the adjacent tissues is about 8 to 1 in the reconstructed image. The vertebral column, lungs, and chambers of the heart appear as voids in this image. The image obtained with ^{11}CO-hemoglobin represents the blood distribution in the chambers of the heart, large blood vessels such as the aorta, and in general in the vascular distribution in surrounding tissues. The ^{18}F is mainly concentrated in the vertebral column, ribs, and sternum. The contrast ratio in the reconstructed image between the vertebral column and immediately surrounding regions is about 15 to 1.

In the second set of experiments, positron transverse tomographic sections of another dog were obtained at the level of the eleventh thoracic vertebra. The administration of $H_2{}^{15}O$, $^{13}NH_3$, and ^{11}CO-hemoglobin was carried out in the same manner as described above. The reconstructed images are shown in Figure 10. The $H_2{}^{15}O$ again shows the soft-tissue distribution, whereas $^{13}NH_3$ is concentrated in the liver because of the incorporation of the ammonia into the urea cycle. The ^{11}CO-hemoglobin displays the blood distribution in large blood vessels, the liver, and the spleen. The large voids are the stomach and small intestine.

The above animal studies were performed without phasic data collection with respect to cardiac cycles or respiration. The only image manipulation was a 4-point nearest-neighbor smoothing of a 64 × 64 data display array. No lower or upper level suppression techniques were employed. The displayed images represent the total reconstructed data. The anatomical structure of the cross sections was verified by lateral and anteroposterior radiographs and by autopsy performed on the second dog.

DISCUSSION

The above results show that positron-emission transaxial tomographic reconstruction permits the visualization of structures which are not ordinarily perceptible with conventional nuclear medicine imaging devices. This result is achieved by the high contrast and uniform resolution inherent in annihilation coincidence detection and by the removal of superposition of structures through the use of mathematical reconstruction. These improvements are important in nuclear medicine, where differences in image contrast determine whether or not a structure is visualized.

The phantoms and animal sections imaged in this study had an outer diameter which did not exceed 20 cm because of the limited transverse field size of the prototype PETT. However, annihilation coincidence imaging can be applied to considerably larger objects, because this method yields resolution and sensitivity independent of depth (Figs. 3 and 4). This is in contrast to single-photon imaging systems which generally exhibit a decreasing resolution with depth. The attenua-

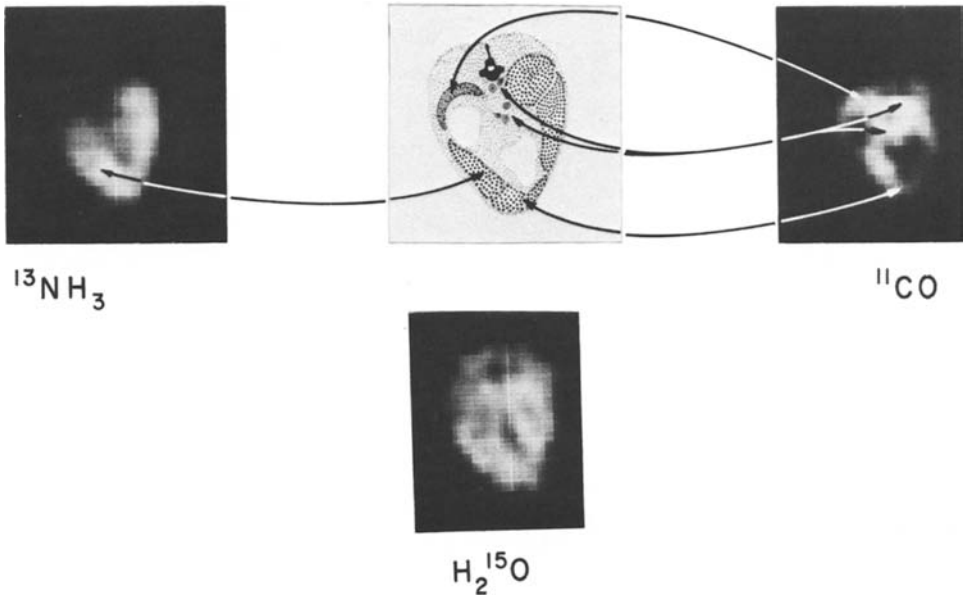

Fig. 10. Cross-section images by the PETT of a dog injected with $H_2{}^{15}O$, $^{13}NH_3$, and ^{11}CO containing 55,000, 205,000, and 232,000 total counts, respectively. The level of the cross section is at the eleventh thoracic vertebra. Anatomical structures at this level which are shown at top center are: spleen (upper left), large blood vessels (center), liver (lower left and upper right).

tion correction of an annihilation coincidence system is simple and accurate. The approximate and more complicated schemes necessary for single photon detection systems must take into consideration the depth dependence and geometrical divergence of the collimated field of view. These problems are amplified for the single-photon counting system as the object size increases. Even if proper attenuation corrections are possible in single photon counting systems, the lower contrast ratio from deep-seated structures requires a large attenuation correction on less well defined structures. The approximations used to correct for these factors, or ignoring them, results in a distortion of the image in single-photon counting systems. The degree of such distortion and its significance in reconstructed images have not yet been fully investigated.

The positron emission transverse tomograph can be designed to utilize the radiation emitted by radionuclides more efficiently than is generally possible with single photon detection systems. The prototype PETT described in this work employs only coincidences occurring in directly opposing pairs of detectors. However, as previously discussed, a much more efficient utilization of the annihilation radiation is accomplished by the use of a multiple coincidence logic. The multiple coincidence logic for the PETT utilizes coincidences between each detector on one side of the hexagon with all the detectors on the opposing side. Thus where the directly opposing coincidence logic uses 12 pairs of coincident detectors, the multiple coincidence has a total of 48, an improvement in efficiency by about a factor of 4. We are presently constructing an enlarged version of the PETT with 8 detectors per side (48 detectors total) and capable of providing a total number of 192 pairs of detectors in coincidence. Since at present the sensitivity of the prototype PETT is comparable to that of a scintillation camera (TABLE I), the newer device should provide a tomographic imaging system considerably faster than conventional cameras presently used in nuclear medicine.

The fact that the PETT can be employed only for radionuclides decaying by positron emission may appear to limit severely the possible clinical usefulness of this approach. However, there are a number of positron-emitting radionuclides with physical and chemical characteristics very favorable for use in nuclear medicine. For example, ^{68}Ga ($T_{1/2}$ = 68 min.) is produced by a long-lived generator, ^{68}Ge ($T_{1/2}$ = 272 days), and is a positron-emitting analog of ^{67}Ga, the usefulness of which is well recognized in nuclear medicine. In addition, a number of nuclides (*e.g.*, ^{11}C, ^{15}O, ^{13}N, ^{18}F) currently employed in physiological studies are positron-emitters. In general, the dedication of this apparatus to the use of positron-emitting radionuclides may be less restrictive than the limitations imposed on scintillation cameras, which require low-energy photon-emitters, or those imposed by the chemical properties of technetium.

It is our opinion that the use of a transaxial tomographic system for the imaging of organs and structures containing positron-emitting radionuclides opens fruitful new areas of exploration in nuclear medicine by removing some of the

restrictive barriers imposed by present-day techniques, instrumentation, and limited choice of radionuclides.

ACKNOWLEDGMENTS: Our thanks are due to Dr. J. R. Cox and Dr. Donald Snyder for algorithms and discussion, to Dr. Henry Huang for simulation and discussions, to Dr. Barry Siegel and Dr. R. E. Coleman for animal preparation and helpful discussions, to Mr. Julius Hecht for technical assistance, and to Ms. Carol Coble for computer programming.

Division of Radiation Sciences
Mallinckrodt Institute of Radiology
Washington University School of Medicine
510 South Kingshighway
St. Louis, Mo. 63110

REFERENCES

1. Beck RN: Collimation of gamma rays. [In] Fundamental Problems in Scanning, ed by A Gottschalk and RN Beck. Springfield, Ill., Thomas, 1968, pp 71–92
2. Beck RN: A theoretical evaluation of brain scanning systems. J Nucl Med **2**:314–324, [Oct] 1961
3. Bowley AR, Taylor CG, Causer DA, et al: A radioisotope scanner for rectilinear, arc, transverse and longitudinal section scanning: (ASS—the Aberdeen section scanner). Brit J Radiol **46**:262–271, Apr 1973
4. Bracewell R, Riddle A: Inversion of fan-beam scans in radio astronomy. Astrophys J **150**:427–434, 1967
5. Brownell GL: Theory of radioisotope scanning. Int J Appl Rad Isotopes **3**:181–192, Aug 1958
6. Brownell GL, Burnham CA, Silensky S, et al: New developments in positron scintigraphy and the application of cyclotron-produced positron emitters. [In] Proc Symp Med Radioisotope Scintigraphy, Salzburg, 6–15 Aug 1968. Vienna, IAEA, 1968, pp 163–176
7. Brownell GL, Sweet WH: Localization of brain tumors. Nucleonics **11**:40–45, 1953
8. Budinger TF, Gullberg GT: Three dimensional reconstruction in nuclear medicine by iterative least-squares and Fourier transform techniques. Donner Lab Rep LBL-2146, Jan 1974
9. Burnham CA, Brownell GL: A multicrystal positron camera. IEEE Med Sci NS19 **3**:201–205, 1973
10. Chesler DA: Positron tomography and three dimensional reconstruction techniques. Proc Symp Radionuclide Tomography, New York, 1972
11. Chesler DA: Three-dimensional activity distribution from multiple positron scintigraphs (abst). J Nucl Med **12**: 347–348, Jun 1971
12. Clarke LP, Laughlin JS, Mayer K: Quantitative organ-uptake measurement. Radiology **102**:375–382, Feb 1972
13. Cormack AM: Reconstruction of densities from their projections, with applications in radiological physics. Phys Med Biol **18**:195–207, 1973
14. Dyson NA: The annihilation coincidence method of localizing positron-emitting isotopes, and a comparison with parallel counting. Phys Med Biol **4**:376–390, Apr 1960
15. Genna S, Farmelant M, Burrows BA: Improved scinti-scan resolution without sensitivity loss: "Constant resolution" collimator. [In] Medical Radioisotope Scintigraphy, Vol. I. Vienna, IAEA, 1968, pp 561–574
16. Gilbert PF: The reconstruction of a three-dimensional structure from projections and its application to electron microscopy. II. Direct methods. Proc R Soc Lond [Biol] **182**: 89–102, 25 Jul 1972
17. Gordon R, Bender R, Herman GT: Algebraic reconstruction techniques (ART) for three-dimensional electron microscopy and x-ray photography. J Theor Biol **29**:471–481, Dec 1970
18. Gordon R, Herman G: Reconstruction of pictures from their projections. Comm ACM **14**:759, 1971
19. Harper PV, Lathrop KA, Krizek H, et al: Clinical feasibility of myocardial imaging with $^{13}NH_3$. J Nucl Med **13**: 278–280, Apr 1972
20. Kuhl D: Section scanning. [In] Proc Symp Soc Nucl Med, New York, 1972. In press
21. Kuhl DE, Edwards RQ: Image separation radioisotope scanning. Radiology **80**:653–661, Apr 1963
22. Kuhl DE, Edwards RQ: Reorganizing data from transverse section scans of the brain, using digital processing. Radiology **91**:975–983, Nov 1968
23. Kuhl DE, Edwards RQ: The Mark III scanner: a compact device for multiple-view and section scanning of the brain. Radiology **96**:563–570, Sep 1970
24. Kuhl DE, Edwards RQ, Ricci AR, et al: Quantitative section scanning using orthogonal tangent correction. J Nucl Med **14**:196–200, Apr 1973
25. Matthews CME: Comparison of coincidence counting and focusing collimators with various isotopes in brain tumour detection. Br J Radiol **37**:531–543, Jul 1964
26. Monahan WG, Tilbury RS, Laughlin JS: Uptake of ^{13}N-labeled ammonia. J Nucl Med **13**:274–277, Apr 1972
27. Myers MJ, Keyes WI, Mallard JR: An analysis of tomographic scanning systems. IAEA-SM-164/48, pp. 331–345
27*a*. Phelps ME, Hoffman EJ, Ter-Pogossian MM: The application of annihilation coincidence detection to transaxial reconstruction tomography. In press.
28. Ramachandran GN, Lakshminarayanan AV: Three-dimensional reconstruction from radiographs and electron micrographs: application of convolutions instead of Fourier transforms. Proc Natl Acad Sci USA **68**:2236–2240, Sep 1971
29. Robertson JS, Marr RB, Rosenbaum M, et al: Thirty-two crystal positron transverse section detector. [In] Tomographic Imaging in Nuclear Medicine, ed by GS Friedman. New York, Soc Nucl Med 1973, pp 142–153
30. Smith P, Peters T, Bates R: Image reconstruction from finite numbers of projections. J Phys A: Math, Nucl Gen **6**: 361–382, 1973
31. Tanaka E: Multi-crystal section imaging device and its data processing. Proc XIII Int Cong Radiol Madrid, 15–20 Oct 1972
32. Tanaka E, Shimizu T, Iinuma T, et al: Digital simulation of section image reconstruction. Nat Inst Radiol Sci (Japan) Rep NIRS-12, 1973, pp 3–4
33. Todd-Pokropek AE: The formation and display of section scans. Proc Symp Amsterdam European Cong Radiol 1971: Radiol Exc Med Amsterdam 1972
34. Todd-Pokropek AE: Tomography and the reconstruction of images from their projections. [In] Proc 3d Int Conf Data Handling and Image Processing, Boston, June 1973
35. Wrenn FR Jr, Good ML, Handler P: The use of positron-emitting radioisotopes for the localization of brain tumors. Science **113**:525–527, 4 May 1951